Pis'ma v ZhETF, vol. 102, iss. 9, pp. 695 – 700

Decay and double-decay properties of edge bands of phosphorene ribbons

M. Yang[1)], *H.-J. Duan, R.-Q. Wang*

Guangdong Provincial Key Laboratory of Quantum Engineering and Quantum Materials, School of Physics and Telecommunication Engineering, South China Normal University, 510006 Guangzhou, China

Submitted 16 September 2015

Phosphorene (a mono-layer of black phosphorus) recently spurred much attention due to its potential for application. We notice there are two types of zigzag edge and also two types of armchair edge for phosphorene lattice. We study the winding number of various types of edge of phosphorene ribbons and conclude that, besides on the typical zigzag edge, the flat zero-energy edge band can be found in the ribbon of another nontypical armchair edge. The localization of these edge bands is investigated analytically. We find every single edge state of the nontypical armchair edge decays to the bulk at two different decay rates.

DOI: 10.7868/S0370274X15210080

I. Introduction. Few-layered back phosphorus was exfoliated from its bulk counterpart Recently [1] and immediately drawn much attention due to its great potential for application. Phosphorene, a mono-layer of back phosphorus, is regarded as a very promising monolayer material for its excellent electronic and mechanic properties. It is expected to be a large-gapped material with high carrier mobility. Phosphorene field-effect transistors have large on-off current ratio at room temperatures [1, 2], and keep high electric quality for long time [3, 4]. The phosphorene lattice has puckered structure, which results in the band structure, collective excitations, and optical response exhibit strong anisotropy [5–8], and phosphorene fragments could be jointed to construct nanotubes without extra energy penalty [9]. Phosphorene sheet is very flexible and can sustain large strain [10], which makes it possible to modify the energy gap and optic properties by applying strain [11–13].

Several papers reported there exist edge states localized at edges of phosphorene ribbons [14–20], and the topologic origin of the edge band of zigzag edge of phosphorene was discussed recently [16]. Unlike the lattices of graphene, silicene, and metal dichalcogenides [21–23], the projection of phosphorene lattice on the layer plane is a deformed honeycomb lattice (see Fig. 1). Due to the lack of 120° rotating symmetry of the phosphorene lattice, there are two types of zigzag edge, as shown in Figs. 2a and b, referred as typic and asymmetric zigzag edges in this paper, and also two types of armchair edge, as in Figs. 3a and b, referred as typic and asymmetric armchair edges. In previous literatures, only the edge bands for the two typic edges were investigated and other two nontypical edges were not noticed. In this paper, we analysis the winding number of a variety of edges of phosphorene ribbons. We find that, besides on the typical zigzag edge, the flat edge band can be found on the asymmetric armchair edge. The localization properties of the edge bands are investigated and the analytical expression of the localization length is obtained. Interestingly, the localization of the edge band of asymmetric armchair edge is governed by two different decay rates, which was verified by the comparison between the analytical results and the tight-binding numerical calculations.

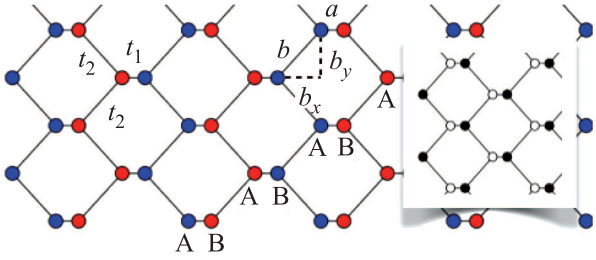

Fig. 1. (Color online) Sketch of phosphorene lattice. The puckered up and down atoms are represented by red- and blue-filled circles. The inset elucidates the phosphorene lattice consisting of two sublattices, where the empty and filled circles denote the sites belong to sublattices A and B respectively

II. Lattice parameters and bulk Hamiltonian. The phosphorene lattice is illustrated in Fig. 1 with relevant quantities labelled in it. The in-plane geometric lattice parameters are $a = 0.8\,\text{Å}$, $b_x = 1.52\,\text{Å}$, and

[1)]e-mail: yang.mou@hotmail.com

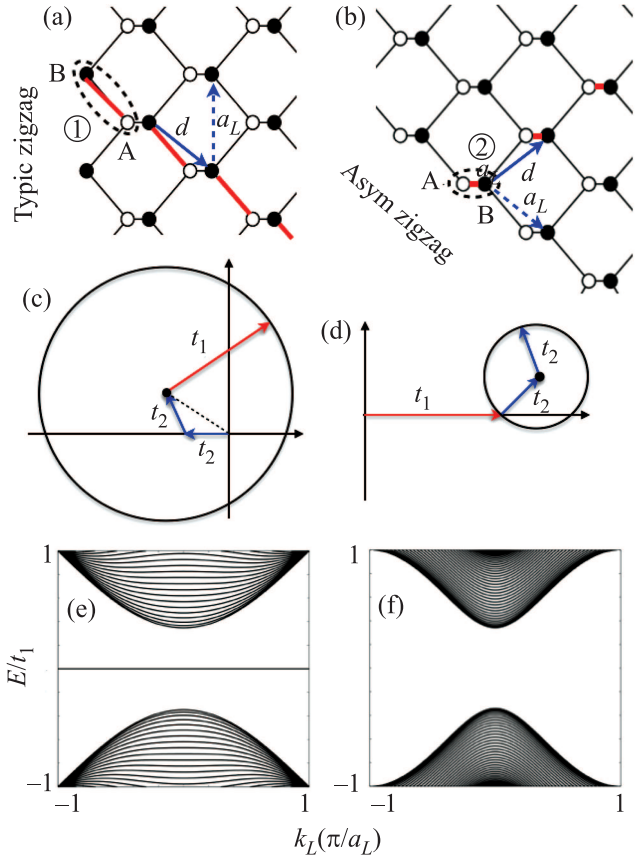

Fig. 2. (Color online) Sketches of typical zigzag and asymmetric zigzag edges of phosphorene, images of the winding number for the two edges, and the band structures of phosphorene ribbons with the corresponding edges

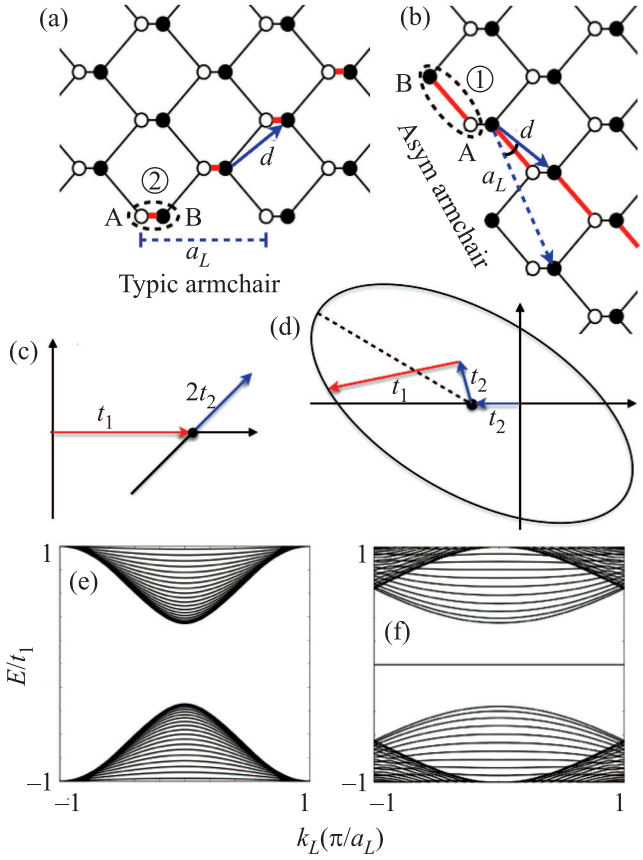

Fig. 3. (Color online) Sketches of typical armchair and asymmetric armchair edges of phosphorene, images of the winding number for the two edges, and the band structures of phosphorene ribbons with the corresponding edges

$b_y = 1.68$ Å [17]. Recent ab-init calculations revealed that the electronic structures can be well described by the tight-binding model with five hopping parameters [8]. Among these parameters, the nearest-neighbor hopping terms, $t_1 = 3.665$ eV and $t_2 = -1.22$ eV, are the largest ones [8], and the other terms also have apparent impact on the electronic structures. Because there is no difference between the on-site energies of the puckered up and puckered down atoms, the atom puckering can be ignored if we are only concerned with the electronic structure [16], and the lattice can be viewed as a composite one consisting of two sublattices, named by A and B (see Fig. 1). As Ref. [16] argued, considering the nearest-neighbor hoppings are enough to explore the topological origin of the edge bands. For these reasons, we only use the nearest-neighbor hoppings to study the edge bands and all calculations are based on the on-plane projection of the phosphorene lattice.

In k-space, by choosing a dimer to study, the bulk Hamiltonian (in basis of either A–B or B–A sublattices) and the dispersion can be obtained as the form

$$H = \begin{bmatrix} 0 & h(k)^* \\ h(k) & 0 \end{bmatrix}, \quad E(k) = \pm|h(k)|, \tag{1}$$

where h depends on the explicit dimer choice. In the following, we will specify h to study the edge bands.

III. Winding number. *1. Zigzag edges.* Winding number reflects the number of edge band, and can be deduced from the bulk Hamiltonian. To deduce the winding number, one have to choose a proper dimer for an individual type of edge. By displacing the dimer, the whole semi-infinite lattice should be completely traversed.

For the typical zigzag edge shown in Fig. 2a, we can choose dimer *1* to construct the bulk Hamiltonian. Displacing dimer *1* by inter times of vector d (transversal displacement vector) forms a dimer-chain, and displacing the dimer-chain by integer times of vector a_L (longitudinal displacement vector) to traverse the lattice. In basis of B–A sublattices, we have h as

$$h = t_2 + t_2 e^{-2ik_y d_y} + t_1 e^{-ik_y d_y} e^{ik_x d_x} = \\ = t_2 + t_2 e^{-ik_L a_L} + t_1 e^{iqd}, \tag{2}$$

where k_L and q are the wavevectors along a_L and d directions, respectively, $d_x = a + b_x$ and $d_y = b_y$ are the x- and y-components of d. In the equation, the relation $qd = k_x d_x - k_y d_y$ is used. In language of winding number, the transversal wavevector q evolutes through out the Brillouin zone while the longitudinal wavevector k_L is fixed as a parameter. During this process, h as a complex number evaluates a closed curve on the complex plane, and the number of turns enclosing the origin is called the winding number. h as a complex vector consists of three vectors representing the three terms in the second line of Eq. (2). When q changes, the first one t_2 lies still along the negative real axis (note $t_2 < 0$), the second one is also static and of the amplitude $|t_2|$ of the orientation depending on k_L, and the third of the amplitude $|t_1|$ rotates circularly. Fig. 2c illustrates the trajectory of h on the complex plane. The ratio

$$\alpha = -\frac{2t_2}{t_1} \tag{3}$$

plays important role to determine the winding number. Because $\alpha = 0.66 < 1$, for whatever relative orientation between the first and the second vectors, or for any k_L, the circle encloses the origin, and the winding number is 1. This manifests that an edge band exists in the whole Brillouin zone. Fig. 2e shows the band structure of a phosphorene ribbon of typical zigzag edge. The edge band can be found as the flat dispersion in the figure.

For the asymmetric zigzag edge in Fig. 2b, dimer *2* is the proper dimer. In basis of A–B sublattices (we always let the leftmost site of the dimer be the first), we have h as

$$\begin{aligned} h &= t_1 + t_2 e^{-ik_y d_y} e^{ik_x d_x} + t_2 e^{ik_y d_y} e^{ik_x d_x} = \\ &= t_1 + t_2 e^{ik_L a_L} + t_2 e^{iqd}, \end{aligned} \tag{4}$$

where the relations $k_L a_L = k_x d_x - k_y d_y$ and $qd = k_x d_x + k_y d_y$ are used. In the second line of the equation, the first one t_1 is a static pointing to the positive real axis, the second one is static one of the amplitude $|t_2|$, and the third rotates a round when q changes through out the Brillouin zone, as Fig. 2d shows. The band structure of phosphorene ribbon of this type of edge can be found in Fig. 2f, in which no edge band exists.

2. Armchiar edges. Now we turn to the armchair edges. The two types of armchair edge, the typical type and asymmetric one, for the phosphorene lattice are illustrated in Figs. 3a and b.

For the typical armchair edge, dimer *2* is the proper selection (see Fig. 3a) for winding number analysis. In basis of A–B sublattices, we have h

$$\begin{aligned} h &= t_1 + t_2 e^{-ik_y d_y} e^{ik_x d_x} + t_2 e^{ik_y d_y} e^{ik_x d_x} = \\ &= t_1 + 2t_2 \cos(qd - k_x d_x) e^{ik_x d_x}, \end{aligned} \tag{5}$$

in which $qd = k_x d_x + k_y d_y$ is used. In the second line of the Eq. (5), h consists of two vectors. The first is a static vector t_1, and when q varies the amplitude of the second vector changes while its orientation is fixed and depends on k_x. The trajectory of h is reduced into a line, as Fig. 3c shows, and so the winding number is zero. The band structure of armchair phosphorene ribbon can be found in Fig. 3e, in which no edge band arises.

For the asymmetric armchair edge, dimer *1* is the proper choice (see Fig. 3b) for the winding number. We have

$$\begin{aligned} h &= t_2 + t_2 e^{-2ik_y d_y} + t_1 e^{-ik_y d_y} e^{ik_x d_x} = \\ &= t_2 + e^{\frac{i}{2}k_L a_L} (t_2 e^{-iqd + \frac{i}{2}k_L a_L} + t_1 e^{iqd - \frac{i}{2}k_L a_L}), \end{aligned} \tag{6}$$

where the relations $qd = k_x d_x - k_y d_y$ and $2k_y d_y = qd - k_L a_L$ are used. The two terms in the brackets in Eq. (6) are two reversely rotating ones when q evolves through, and form an ellipse with the minor and major radiuses being $|t_1 + t_2|$ and $|t_1 - t_2|$, respectively (the major radius orientates vertically). The pre-factor before the brackets makes the orientation of the ellipse tilted. The first term t_2 determines the location of the ellipse center, which is on the negative real axis. Because the minor radius is larger than the distance between the ellipse center and the origin, i.e., $|t_1 + t_2| > |t_2|$ (equivalently, $\alpha < 1$), the origin is included in the ellipse, and the winding number is 1. The imaging of the winding number is illustrated in Fig. 3d, and the band structure of the phosphorene ribbon is shown in Fig. 3f.

IV. Localization of edge bands. The localization of the edge bands is often obtained by solving the Shrödinger function on the lattice sites, as Ref. [24] does. Indeed, this is unnecessary. The edge bands in Figs. 2f and 3f (also in Figs. 4a and b) are flat zero energy bands. To ensure the energy being zero, we simply let

$$h = 0, \tag{7}$$

and it is enough to extract the localization properties. For the typical zigzag ribbon, h is given in Eq. (2), and the restriction results in

$$t_2 + t_2 e^{-2ik_y d_y} + t_1 e^{-ik_y d_y} e^{ik_x d_x} = 0. \tag{8}$$

This equation leads to

$$e^{ik_x d_x} = \alpha \cos k_y d_y, \tag{9}$$

where α is the ratio defined in Eq. (3). This equation cannot be satisfied for k_x and k_y being real simultaneously. Because k_y is the longitudinal wavevector and it

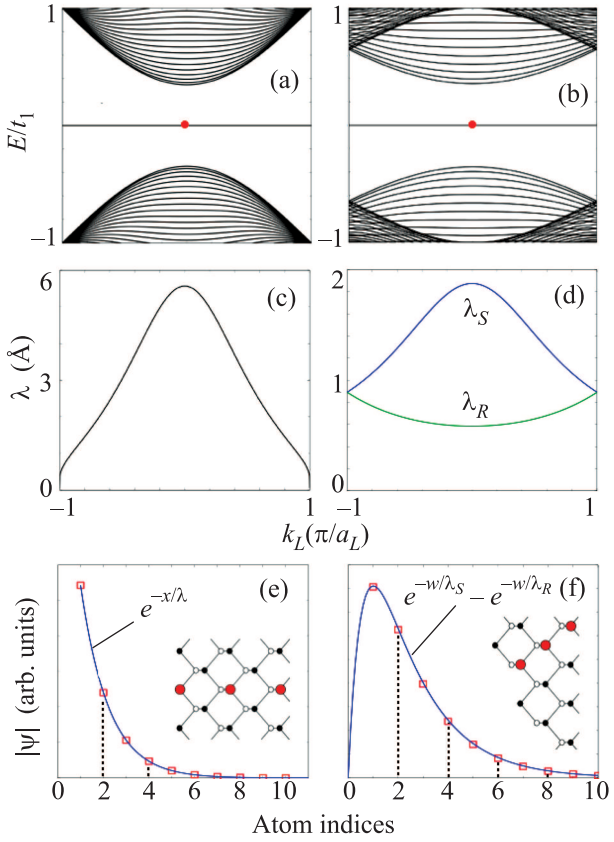

Fig. 4. (Color online) (a) b) – Band structures of phosphorene ribbons of typical zigzag and assymetric armchair edges. (c, d) – Wavefunction localization lengths of edge band states as functions of wavevector k_L. (e, f) – Wavefunction amplitude of the edge states (labeled by the bold dots in a and b) on the atom lines indicated in the insets, where the square marks are obtained by tight-binding calculations

is real, k_x must be imaginary. The imaginary wavevector k_x determines the localization of the edge states. By denoting $\kappa_x = |k_x|$ and replacing $ik_x d_x$ with $-\kappa_x d_x$, we have

$$\kappa_x = -\frac{1}{d_x}\ln(\alpha\cos k_y d_y). \tag{10}$$

This equation tells the rate of the edge state decaying to the bulk. By defining the wavefunction localization length λ, we have

$$\lambda = \frac{1}{\kappa_x} = -\frac{d_x}{\ln(\alpha\cos k_y d_y)}. \tag{11}$$

Fig. 4c shows the localization length as a function of k_L ($k_L = k_y$ for this case). The band structure of the zigzag ribbon is also listed in the figure to make the problem more clear. The localization depends on the energy difference between the edge band and the bulk band. The smaller difference means the weaker localization. Among all the edge states of k_L, the least localized state is the one of $k_L = 0$, and its localization length reads

$$\lambda_{\max} = -\frac{d_x}{\ln\alpha}. \tag{12}$$

For the adopted parameters, $\lambda_{\max}$ is about several Å, which means that the wavefunction can only be found on a few slices of sites near the edge. The most localized state is the one of $k_y = \pi/a_L = \pi/2d_y$ (or equivalently, $-\pi/a_L$), the localization length of which is

$$\lambda_{\min} = 0. \tag{13}$$

This manifests that the state is completely localized on these outmost sites. The wavefunction amplitude of the edge bandcan only found nonzero on B-type sites (or A-type sites near the opposite edge) and it is

$$|\psi_{\mathrm{B}}| \sim e^{-x/\lambda}. \tag{14}$$

Fig. 4e shows both the analytical and numerical tight-binding results of the wavefunction amplitude on the line of sites labeled in the inset.

For the asymmetric armchair edge, h is given in Eq. (6), and the zero energy restriction requires

$$t_2 + e^{\frac{i}{2}k_L a_L}(t_2 e^{-iqd+\frac{i}{2}k_L a_L} + t_1 e^{iqd-\frac{i}{2}k_L a_L}) = 0. \tag{15}$$

This equation gives the relation q as the function of k_L. In general, q is not a real number and consists of an imaginary part, which determines the decay properties of the edge band. By denoting the decay rate in d-direction as κ, after a little bit derivation (see Appendix A), we find that, for one k_L, there are two allowed values of κ, a rapid decay rate κ_R and a slow one κ_S, determined by

$$\begin{aligned}\kappa_R d &= -\ln\beta + \frac{\beta}{2}\cos\left(\frac{1}{2}k_L a_L\right),\\ \kappa_S d &= -\ln\beta - \frac{\beta}{2}\cos\left(\frac{1}{2}k_L a_L\right),\end{aligned} \tag{16}$$

where β is a dimensionless factor defined by

$$\beta = \left(-\frac{t_2}{t_1}\right)^{1/2}, \tag{17}$$

which describes the asymmetry between the two ends of dimer *1* in Fig. 3b. For the phosphorene lattice, $\beta = 0.56$. The localization length along d-direction is $1/\kappa$, thus the localization lengths in the direction normal to the edge, λ_R for rapid decay and λ_S for slow decay, are

$$\lambda_R = \frac{\sin\theta}{\kappa_R}, \quad \lambda_S = \frac{\sin\theta}{\kappa_S}, \tag{18}$$

where θ is the angle of vector d with respective to the longitudinal direction, which can be worked out by $\sin\theta = 2d_x d_y/(a_L d)$ with $a_L = \sqrt{d_x^2 + (3d_y)^2}$. Fig. 4d shows the localization lengths λ_R and λ_S as functions of k_L. The localization lengths at $k_L = 0$ are

$$\lambda_S(0) = \frac{d\sin\theta}{-\ln\beta - \beta/2}, \quad \lambda_R(0) = \frac{d\sin\theta}{-\ln\beta + \beta/2}. \tag{19}$$

At the ends of the Brillouin zone, the two localization lengths are reduced into a single one, namely,

$$\lambda_S(\pi/a_L) = \lambda_R(\pi/a_L) = -\frac{d\sin\theta}{\ln\beta}. \tag{20}$$

The edge state at $k_L = \pi/a_L$ can be viewed as the most localized state. Unlike the typical zigzag edge, the localization length of it is nonzero. The wavefunction amplitude of the edge band on B-type sites is governed by the combination of two decay terms,

$$|\psi_{\rm B}| \sim e^{-w/\lambda_S}, e^{-w/\lambda_R}, \tag{21}$$

where w denote the coordinate along the direction normal to the edge. To check the validity of the double-delay feature, we compare the numerically tight-binding and analytically calculated wavefunction amplitude on the line of sites labeled in the inset of Fig. 4f. The relative weight between the two different decays is determined by the edge condition of the wavefunction, which is elucidated in Appendix B. As Fig. 4f shows, the two calculation methods coincide.

V. Summary. We studied the topological origin of the edge band of phosphorene ribbon of various edges by means of the winding number. By simply using the zero energy constriction of the edge bands, we obtained the analytic expressions of localization lengths of the edge states. The double-decay feature is found for the edge band of the asymmetric armchair edge.

This work was supported by NSF of China Grant # 11274124, 11474106, and 11174088.

Appendix A. Derivation of Eq. (16). Following the second line of Eq. (6), h can be deformed into

$$t_2 + |t_1 t_2|^{\frac{1}{2}} e^{\frac{i}{2}k_L a_L}\left(-\beta e^{-iqd+\frac{i}{2}k_L a_L} + \beta^{-1} e^{iqd-\frac{i}{2}k_L a_L}\right), \tag{A1}$$

where β is the quantity defined by Eq. (17). By noticing $\beta = e^{\ln\beta}$, the above expression can be reduced to

$$t_2 + 2|t_1 t_2|^{\frac{1}{2}} e^{\frac{i}{2}k_L a_L}\sinh\left(iqd - \frac{i}{2}k_L a_L - \ln\beta\right). \tag{A2}$$

The restriction of zero energy leads to the equation

$$-\beta + 2e^{\frac{i}{2}k_L a_L}\sinh\left(iqd - \frac{i}{2}k_L a_L - \ln\beta\right) = 0. \tag{A3}$$

We rewrite the equation as

$$\frac{\beta}{2}e^{-\frac{i}{2}k_L a_L} = \sinh\left(iqd - \frac{i}{2}k_L a_L - \ln\beta\right), \tag{A4}$$

and we have

$$iqd = \operatorname{arcsinh}\left(\frac{\beta}{2}e^{-\frac{i}{2}k_L a_L}\right) + \frac{i}{2}k_L a_L + \ln\beta. \tag{A5}$$

The wavevector q consists real and imaginary parts, only the imaginary part corresponds to the decay of the wavefunction. Denoting imaginary part as κ, we have

$$-\kappa d = \operatorname{Re}(iqd). \tag{A6}$$

Only keep the real part of Eq. (A5), and we have

$$\kappa d = -\ln\beta - \operatorname{Re}\left[\operatorname{arcsinh}\left(\frac{\beta}{2}e^{-\frac{i}{2}k_L a_L}\right)\right]. \tag{A7}$$

In the equation, k_L and $k_L + 2\pi/a_L$ represent the same quantum state, but they result in two different value of κ because $\operatorname{arcsinh}(e^{ix}) = -\operatorname{arcsinh}[e^{i(x+\pi)}]$. That is to say, we have two decay rates for a single state labeled by k_L:

$$\kappa_{R/S} d = -\ln\beta \pm \operatorname{Re}\left[\operatorname{arcsinh}\left(\frac{\beta}{2}e^{-\frac{i}{2}k_L a_L}\right)\right] \approx$$
$$\approx -\ln\beta \pm \frac{\beta}{2}\cos\left(\frac{1}{2}k_L a_L\right). \tag{A8}$$

So we have Eq. (16). In the above equation, the valid of the approximation relies on the fact $\beta/2 = 0.29 \ll 1$.

Appendix B. Wavefunction on a line of sites. The line of sites labeled in Fig. 4f is normal to the edge direction. The wavefunction on the line is governed by two decay rates, and the explicit form depends on the edge condition. Suppose there is an virtual B-type site on the line before the leftmost site, the virtual site is a site directly connected to the ribbon edge, and cutting it apart from the ribbon edge means the wavefunction on it must be zero. In the continuum limit, the edge condition of wavefunction of B-type sites along the line can be expressed as

$$\psi_{\rm B}(w = 0) = 0. \tag{B1}$$

After considering this condition, we have the wavefunction the on the atom line,

$$\psi_{\rm B} = C(e^{-w/\lambda_S} - e^{-w/\lambda_R}), \tag{B2}$$

where C is the normalization constant. So, we have Eq. (21) and the expression in Fig. 4f.

1. F. Xia, H. Wang, and Y. Jia, Nat. Commun. **5**, 4458 (2014).
2. L. Li, Y. Yu, G. Ye, Q. Ge, X. Ou, H. Wu, D. Feng, X. Chen, and Y. Zhang, Nat. Nanotech. **9**, 372 (2014).
3. J. D. Wood, S. A. Wells, D. Jariwala, K.-S. Chen, E. Cho, V. K. Sangwan, X. Liu, L. J. Lauhon, T. J. Marks, and M. C. Hersam, Nano Lett. **14**, 6964 (2014).
4. G. Wang, R. Pandey, and S. P. Karna, Nanoscale **7**, 524 (2014).
5. T. Low, R. Roldán, H. Wang, F. Xia, P. Avouris, L. M. Moreno, and F. Guinea, Phys. Rev. Lett. **113**, 106802 (2014).
6. A. S. Rodin, A. Carvalho, and A. H. Castro, Neto Phys. Rev. B **90**, 075429 (2014).
7. V. Tran, R. Soklaski, Y. Liang, and L. Yang, Phys. Rev. B **89**, 235319 (2014).
8. A. N. Rudenko and M. I. Katsnelson, Phys. Rev. B **89**, 201408(R) (2014).
9. J. Guan, Z. Zhu, and D. Tománek, Phys. Rev. Lett. **113**, 226801 (2014).
10. Q. Wei and X. Peng, Appl. Phys. Lett. **104**, 251915 (2014).
11. H. Guo, N. Lu, J. Dai, X. Wu, and X. C. Zeng, J. Phys. Chem. C **118**, 14051 (2014).
12. A. S. Rodin, A. Carvalho, and A. H. Castro, Neto Phys. Rev. Lett. **112**, 176801 (2014).
13. D. Çakır, H. Sahin, and F. M. Peeters, Phys. Rev. B **90**, 205421 (2014).
14. J. Zhang, H. J. Liu, L. Cheng, J. Wei, J. H. Liang, D. D. Fan, J. Shi, X. F. Tang, and Q. J. Zhang, Sci. Rep. **4**, 6452 (2014).
15. Z. Zhu, C. Li, W. Yu, D. Chang, Q. Sun, and Y. Jia, Appl. Phys. Lett. **105**, 113105 (2014).
16. M. Ezawa, New J. Phys. **16**, 115004 (2014).
17. A. Carvalho, A. S. Rodin, and A. H. C. Neto, Europhys. Lett. **108**, 47005 (2014).
18. A. Maity, A. Singh, and P. Sen, arXiv:1404.2469.
19. X. Peng, A. Copple, and Q. Wei, J. Appl. Phys. **116**, 144301 (2014).
20. M. Yang, H.-J. Duan, and R.-Q. Wang, JETP Lett. **102** 322 (2015).
21. A. H. Castro Neto, F. Guinea, N. M. R. Peres, K. S. Novoselov, and A. K. Geim, Rev. Mod. Phys. **81**, 109 (2009).
22. A. Kara, H. Enriquez, A. P. Seitsonen, L. C. L. Y. Voon, S. Vizzini, B. Aufray, and H. Oughaddou, Surf. Sci. Rep. **67**, 1 (2012).
23. K. F. Mak, C. Lee, J. Hone, J. Shan, and T. F. Heinz, Phys. Rev. Lett. **105**, 136805 (2010).
24. M. Bellec, U. Kuhl, G. Montambaux, and F. Mortessagne, New J. Phys. **16** 113023 (2014).